

ROYAL SOCIETY OPEN SCIENCE

Research



Article submitted to journal

Subject Areas:

computational biology, biomechanics

Keywords:

energy invariant, flight modelling,
motion vision

¹
Author for correspondence:

Julien R. Serres

e-mail: julien.serres@univ-amu.fr

Optic flow helps explain gulls' altitude control over seas

Julien R. Serres¹, Thomas J. Evans^{2,5},
Susanne Åkesson², Olivier Duriez³, Judy
Shamoun-Baranes⁴, Franck Ruffier¹ and
Anders Hedenström²

¹Aix Marseille Univ, CNRS, ISM, Marseille, France

²Dept of Biology, CAnMove, Lund University, Ecology Building, SE-223 62 Lund, Sweden

³CEFE UMR 5175, CNRS - Université de Montpellier - Université Paul-Valéry Montpellier - EPHE – 1919 route de Mende, 34293 Montpellier cedex 5, France

⁴Computational Geo-Ecology, Inst. of Biodiversity and Ecosystem Dynamics, University of Amsterdam, P.O. Box 94 248, 1090 GE Amsterdam, The Netherlands

⁵Marine Scotland Science, Marine Laboratory, 375 Victoria Road, Aberdeen, AB11 9DB, Scotland, UK

For studies of how flying animals control their flight, seabirds are of particular interest to track with a bio-logger because they forage offshore where the visual environment can be simply modeled by a flat world textured by waves. This study suggests that optic flow can explain gull's altitude control over seas. In particular, a new flight model that includes both energy and optical invariants (called the *ventral optic flow regulation*) explain the dynamics of gulls' altitude control during offshore takeoff and cruising flight. A linear statistical model applied to 352 flights from 16 individual lesser black backed gulls (*Larus fuscus*) gave a strong correlation between wind assistance and gulls' altitude. Thereafter, an optic flow-based flight model was applied to 18 offshore takeoff flights from 9 individual gulls. By introducing an upper limit in climb rate in a non-linear first order parametric model on the gull's elevation dynamics, coupled with an optic-flow set-point, the predicted altitude gives an optimized fit factor value of 63% on average (min value: 30%, max value: 83%) with respect to GPS data. We conclude that the optic-flow regulation principle (here running close to 25°/s) allows gulls to adjust their altitude over sea without having to directly measure their current altitude.

2 1. Introduction

2

3 Understanding how a bird decides to fly at a given altitude during a specific manoeuvre is a
 4 difficult task because it is strongly dependent on the atmospheric conditions and flight capacity
 5 of the bird (see review [59]). Seabirds such as albatrosses and petrels flying close to the sea surface
 6 take advantage of the logarithmic increase in wind speeds to support dynamic soaring [50, 52, 53,
 7 66], which works only at very low altitudes from ca. 0-10 m (see e.g. Fig. 5 in [56]). Birds flying by
 8 flapping flight at low altitudes over the sea could also use this windspeed gradient to reduce their
 9 transport costs. Under tailwinds, birds should fly higher where wind speed is high, while under
 10 headwinds birds should fly lower where wind speed is low. In terms of energy, a bird minimizing
 11 its transport cost should adjust its airspeed with respect to wind by increasing it in headwinds
 12 and decreasing it in tailwinds [26, 48]. This prediction comes from a U-shaped function between
 13 power required to fly and airspeed, which defines characteristic speeds for achieving minimum
 14 power V_{mp} and maximum range V_{mr} . During migratory [38] and homing flights [33] birds utilize
 15 wind assistance to minimize the transport cost and adjust airspeed accordingly to fly at the wind
 16 dependent V_{mr} .

17 Groundspeed is the combined effect of airspeed and wind speed (actually the airspeed and
 18 wind vectors). Wind assistance alone cannot be used by the bird to select a given groundspeed

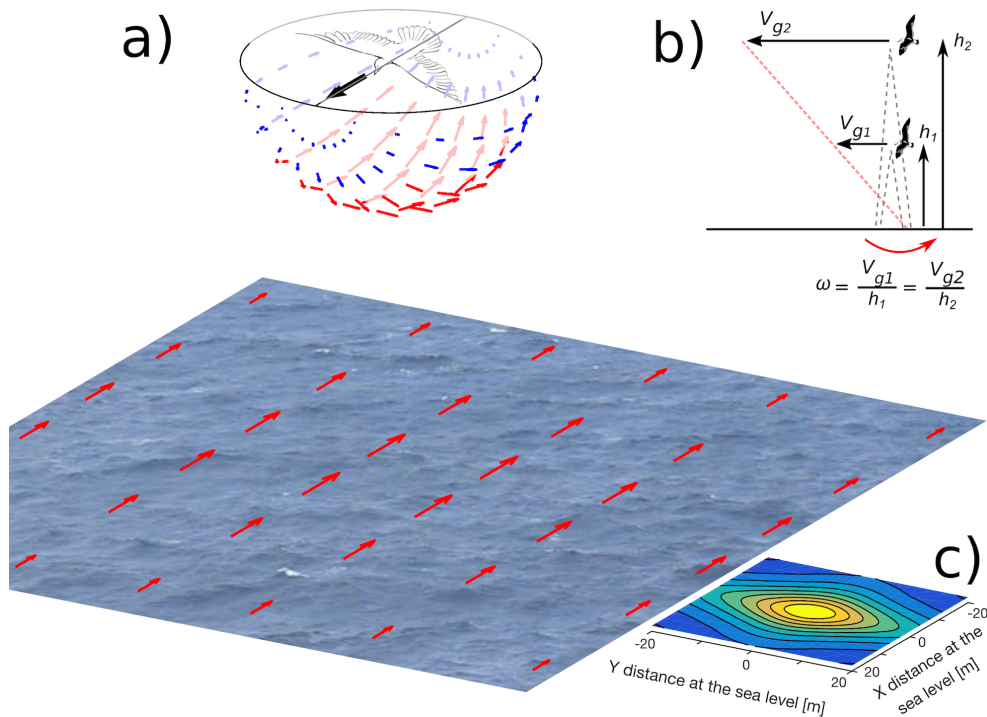


Figure 1. (a) A gull flying over the sea generates a vector field of optic flow. Such a vector field is perceived by a gull based on the contrasts created by waves and white-crested waves (also called white-horses). Inspired by [19]. (b) The magnitude of the vector of the optic flow, ω , is determined by the gull's groundspeed, V_g , and its altitude, h . If ω is held constant by adjusting the altitude, h will always tend (through the bird dynamics) to be proportional to V_g (only a linear combination -red dashed line- between h and V_g is asymptotically possible). (c) Optic flow magnitude in the ventral field of view at 10m-height where the magnitude of the ventral optic flow $\omega(\phi, \theta) = \frac{V_g}{h} \sin^2 \theta \times \cos \phi$ is projected at the sea level with ϕ the azimuthal angle and θ the elevation angle. (The magnitude of vertical optic flow is the maximum and is $\omega(\phi = 0^\circ, \theta = -90^\circ) = \frac{V_g}{h}$)

19 and a flight altitude. The altitude could be set by surrounding visual information seen by
20 the bird. A bird can access information about its own motion with respect to its surrounding
21 environment via the optic flow field through its early visual processing [4], as flying insects do
22 in similar situations [4, 58]. The optic flow field perceived by an agent (a flying insect, a bird,
23 or a human) is particularly dependent on the structure of the environment [19, 35, 45, 67]. Optic
24 flow can be defined by a vector field of the apparent angular velocities of objects, surfaces, and
25 edges in a visual scene caused by the relative motion between the agent and the scene (Fig.
26 1). The translational optic flow component is particularly interesting for birds positioning in
27 space because it depends on (i) the ratio between the relative linear groundspeed of an object
28 in the scene with respect to the bird, and (ii) the distance from obstacles in the surrounding
29 environment. Consequently, optic flow requires neither groundspeed nor distance measurement,
30 which is particularly useful to explain how birds perceive the world because birds are likely
31 unable to sense directly their own groundspeed nor the 3D structure of the environment in which
32 the binocular vision plays a minor role [39].

33 During flight manoeuvres, various optic flow parameters (such as the magnitude, the
34 direction, the focus of expansion, the time-to-contact of optic flow) can be collected by birds to
35 control their lateral position in straight tunnels (in budgerigars [7]), to decrease their speed in
36 a converging tunnel (in budgerigars [57]), to plunge into water (in gannets [36]), to hover (in
37 hummingbirds [20, 54]), and finally to land (in hawks [12] and in hummingbirds [37]).

38 In this study, we address the question of how seabirds control their altitude during offshore
39 takeoffs and cruise flights with respect to wind. Here, two working hypotheses were compared
40 about altitude control:

- 41 • a first hypothesis based on a direct measurement and regulation of optic flow that adjusts
42 the altitude, and,
- 43 • a second hypothesis based on a direct measurement of the barometric pressure that
44 directly regulates the altitude itself.

45 To test these alternative hypotheses, a statistical analysis of 352 flights comprising 16
46 individual lesser black-backed gulls (*Larus fuscus*) in various wind conditions were conducted.
47 Then, 18 offshore takeoffs followed by a cruise flight were analyzed by taking into account
48 morphological parameters from 9 individual gulls.

49 2. Operating point in flight in terms of speed and altitude: a 50 theoretical approach

51 (a) How is bird speed deduced from aerodynamic effects?

52 The relationship between:

- 53 – the bird's ground speed V_g
- 54 – the bird's airspeed V_{air}
- 55 – the wind speed V_w

56 is given by equation (2.1):

$$V_g = V_{air} + V_w \quad (2.1)$$

57 The basis for deriving predictions about bird flight is the so-called flight mechanical theory,
58 which combines the relationship between power output P and airspeed V_{air} in flapping flight as
59 follows:

$$P(V_{air}) = a + b \cdot V_{air}^{-1} + c \cdot V_{air}^3 \quad (2.2)$$

60 where a , b , and c represent various physical, morphological and physiological properties of the
61 bird and air [47, 49, 51]. If the objective is to minimize the energy cost per unit distance (i.e., cost
62 of transport), the optimal flight speed is the maximum range speed V_{mr} [26, 47]. The maximum
63 range speed V_{mr} is obtained from the U-shaped power curve [24, 27, 51] by the condition:

$$\left(\frac{\partial P}{\partial V_{air}} \right)_{V_{air}=V_{mr}} = \frac{P(V_{mr})}{V_{mr}} \quad (2.3)$$

Indeed, a gull's homing flight is similar to a migratory flight, in that it is assumed that the flight's objective is principally for transportation, as opposed to outbound foraging flights when the bird is likely also searching for food. Seabirds' homing flight over the sea is therefore a relatively straight path between two locations. During transport flight gulls are expected to minimise overall energy expenditure or time, thus cost of travel per unit distance should be minimised rather than instantaneous energy expenditure. If minimising the cost of travel per unit distance birds will travel at maximum range speed (V_{mr}) not minimum power airspeed (V_{mp}). V_{mr} refers to V_{air} rather than V_g . If a bird experiences a tailwind, its cost of travel per unit distance decreases, thus V_{mr} also declines. Conversely under headwinds V_{mr} increases. In a recent work, it was analyzed how lesser black-backed gulls (and guillemots) modulate their airspeeds in relation to winds [17]. It was found that gulls increased airspeeds under headwinds and decreased airspeeds under tailwinds [17], and similar behaviour has been observed during longer distance homing flights [42]. These results suggest that gulls are flying at V_{mr} rather than V_{mp} , since V_{mp} should not be affected by winds like V_{mr} [17].

(b) Optic flow vector field

Consider a bird flying over the sea, assumed as flat in the optic flow calculation, then based on groundspeed V_g only (neglecting vertical speed V_z) the magnitude of the ventral optic flow field ω can be expressed as follows:

$$\omega(\phi, \theta) = \frac{V_g}{h} \sin^2 \theta \times \cos \phi \quad (2.4)$$

with h the altitude, θ the elevation angle and ϕ the azimuth angle.

The magnitude of the ventral optic flow field is plotted in Fig. 1a with the projection of its elevation and azimuth angles over the sea. The larger projection of vector magnitude of optic flow over the sea is shown using a contour plot in Fig. 1c in the case of a bird flying at a height of 10 m. The bird may be able to perceive the optic flow maximum from a non-negligible area of its field of view (Fig. 1c). The maximum magnitude of the ventral optic flow is always vertically downwards from the bird in the direction of the sea :

$$\omega(\phi = 0^\circ, \theta = -90^\circ) = \frac{V_g}{h} \quad (2.5)$$

(c) How the model predicts the bird's flight height from the ventral optic flow regulation principle

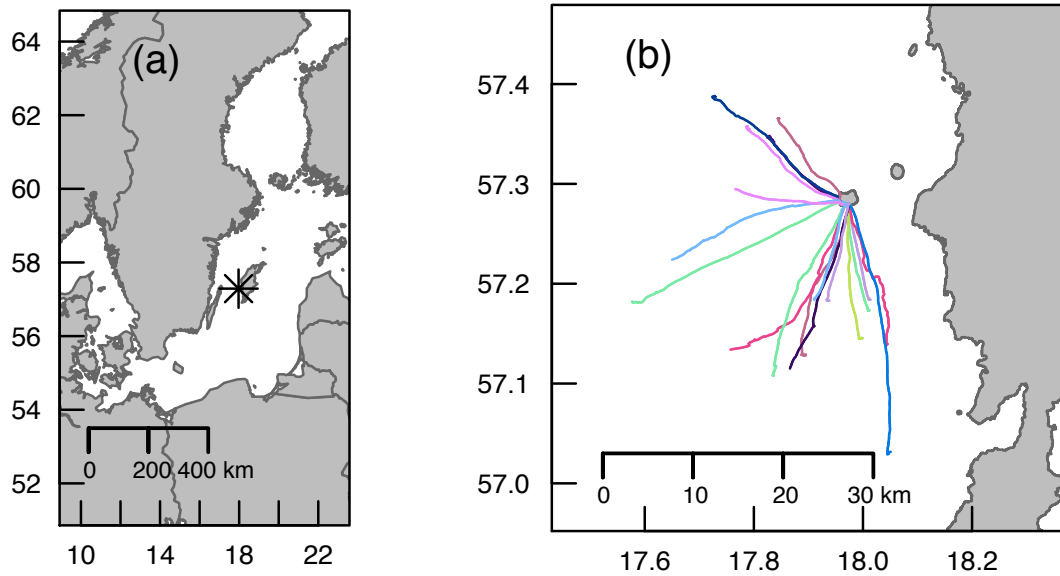
The ventral optic flow regulation principle tends to keep constant the vertically downward optic flow whatever the speed or height of flight by adjusting the altitude [18, 55]. Here, it introduces this asymptotic proportionality relationship for birds: the bird's height of flight h will always tend (through the bird dynamics) to be proportional to the bird's ground speed V_g (Fig. 1b) as :

$$\omega_{sp} = \omega(\phi = 0^\circ, \theta = -90^\circ) = \frac{V_g}{h} = \text{constant} \quad (2.6)$$

where ω_{sp} is the ventral optic flow set-point. Besides, the wind profile power-law is often used to estimate the horizontal wind speed [31] as follows:

$$V_w = V_{ref} \cdot \left(\frac{h}{h_{ref}} \right)^\alpha \quad (2.7)$$

with the parameter α is the power-law exponent (that is usually specified as a function of stability as well as the roughness of the surface $0 < \alpha < 1$ (here over seas $\alpha = 0.11$ see [30]), the speed



5

Figure 2. (a) Study location of the island of Stora Karlsö (indicated by *asterisk), Baltic Sea, Sweden. (b) From this site Lesser Black-backed Gull (*Larus fuscus*) inbound flights were tracked with GPS (18 flights from 9 individual gulls, coloured lines).

99 V_{ref} as being the wind speed at a reference height h_{ref} (10m). By combining (2.6) and (2.7) into
 100 (2.1), we obtain:

$$\omega_{sp} \cdot h = V_{air} + V_{ref} \cdot \left(\frac{h}{h_{ref}} \right)^\alpha \quad (2.8)$$

101 To find the bird's steady-state flight height h reached during a takeoff as function of the wind
 102 profile, it requires to solve the equation $f(h) = 0$ with the function f defined as follows:

$$f(h) = V_{air} + V_{ref} \cdot \left(\frac{h}{h_{ref}} \right)^\alpha - \omega_{sp} \cdot h \quad (2.9)$$

103 In the variation table of the function f (Tab. S1), we observe that only one unique altitude h
 104 exists, enabling $f(h) = 0$ during an offshore takeoff manoeuvre. We can therefore conclude that
 105 both the minimisation of the rate of energy consumption and regulating the ventral optic flow
 106 enable a bird to fix both its groundspeed and its altitude above the sea. The bird's steady-state
 107 flight height h cannot be considered as a "target flight height" or a "desired flight height", but as an
 108 "optimal flight height" because the bird's altitude is adjusted as a function of the wind conditions
 109 (higher under tailwinds but lower under headwinds) and thereby maximizing positive effects as
 110 well as minimizing adverse effects of the wind gradient.

111 3. Gulls' trajectory recording

112 16 lesser black-backed gulls (*Larus fuscus*) were GPS tracked from their breeding colony on Stora
 113 Karlsö island, Sweden (17.972° E, 57.285° N) during May to September of 2013-2015. The island
 114 is a small offshore island (2.5 km²) located in the western central Baltic Sea, sited 7 km west of the
 115 much larger island of Gotland (Fig. 2a). During breeding the gulls perform central-place foraging
 116 trips [46], flying out from their island to forage, either at sea or on land [32].

117 Gulls were caught during late incubation (late May) using walk-in traps set over their nests.
 118 They were weighed and sexed from morphological measurements [11] or genetically [23] from a

119 few breast feathers taken at capture. An 18 g solar-powered UvA-BiTS GPS tracker with remote
120 download capacity [9] was mounted using either a full body or wing harnesses [64] constructed
121 of tubular TeflonTM ribbon (Bally Ribbon Mills 8476-.25") (full tagging procedure given in [32],
122 see Fig. 3). Data were downloaded and programs uploaded to the GPS devices remotely using
123 a network of four antennas providing good coverage of the colony area. GPS tracking was
124 continuous though the location intervals varied depending on the requirements of parallel studies
125 (e.g. [32]). At a 6 seconds interval on a white stork (*Ciconia ciconia*) on its nest, it was quantified a
126 mean altitude error of 2.77 m and a mean speed error of 0.02 m/s of the UvA-BiTS GPS tracker
127 [9].



Figure 3. Lesser black-backed gull (*Larus fuscus*) equipped with an 18 g solar-powered UvA-BiTS GPS tracker (see [9] for GPS tracker details). Photographic credit: the authors.

128 The continuous GPS tracks were segmented into foraging trips and within these, sections of
129 continuous flight, with the final flight of a foraging trip considered a homing flight, as the gulls
130 returned from presumed foraging at sea (only marine trips were used in this study, c.f. [32]) to
131 the island colony. 18 takeoffs from 9 individual gulls with high resolution data were selected (i.e.
132 10 or 15-second intervals), and we selected only takeoffs reaching a steady-state altitude - i.e.
133 not those with a constantly fluctuating altitude. In addition, the final altitude had to be greater
134 than 10 m with variation in altitude during the ascent until reaching a steady-state altitude.
135 Flight GPS points were annotated with wind data extracted from a global weather model, ERA-
136 interim data [13] provided by the European Centre for Midrange Weather Forecasts (ECMWF,
137 <http://www.ecmwf.int/en/research/climate-reanalysis/era-interim>), which gives variables at
138 3-hour intervals and is gridded with a spatial resolution of approximately 79 km. These were
139 extracted using the environmental-data automated track annotation (Env-DATA) system [14]
140 hosted by MoveBank (<http://www.movebank.org/>).

141 4. Full flights' dataset analysis: statistical model

142 The dataset here includes all inbound (returning to the island colony) over sea flights by the lesser
143 black-backed gulls (383 flights, 16 gulls). The dataset is composed of median altitudes h calculated
144 per flight, median wind speed measured at 10m-height (from ECMWF data), V_{ref} , and the gull
145 identifier. After excluding the flights endowed with a median altitude below zero meters, the data
146 comprise 352 observations of 16 individual gulls.

147 A nonlinearity of wind profile power law (2.7) was introduced to estimate the wind speed
148 $V_w(h)$ experienced by gulls at their median altitude h calculated per flight. A linear mixed effect
149 model was designed using *lmer* in R software for the ordinates (β_i is the constant random effect)
150 as follows:

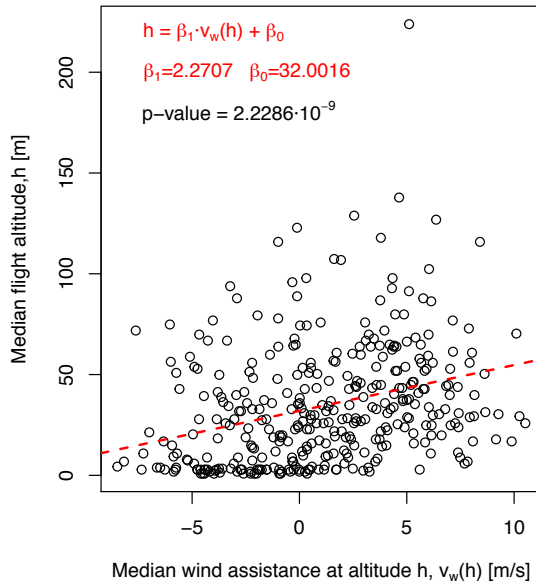


Figure 4. Gull's median altitude h versus median wind assistance V_w (head or tail wind) at median altitude h for 352 flights (16 distinct gulls). The regression line using β_1 and β_0 is plotted in red.

$$h = \beta_1 \cdot V_w(h) + \beta_0 + \beta_i + \varepsilon_{i,V_w} \quad (4.1)$$

151 with the regression parameters: $\beta_1 = 2.2707$ and $\beta_0 = 32.0016$. The Kenward-Roger corrected F-
 152 test was used to calculate the significance level of the linear mixed model (ndf:1, ddf: 347.89, Fstat:
 153 37.722, p.value: $2.2286 \cdot 10^{-9}$, F.scaling: 1). The parameter β_1 was highly significant (Fig. 4). Using
 154 the coefficient $\beta_1 = 2.2707$, an identification of the ventral optic flow set-point $\omega_{sp-lmer}$ can be
 155 performed using the equation (2.8) that includes the wind profile power law as follows:

$$\omega_{sp-lmer} = \frac{1}{\beta_1} = 0.4403 \text{ rad/s} = 25.23^\circ/\text{s} \quad (4.2)$$

156 This statistical analysis tells us that gulls tend to maintain a ventral optic flow close to $25.23^\circ/\text{s}$
 157 whatever the wind conditions are while flying above the sea.

158 5. Takeoff time series analysis: individually tuned parametric 159 model

160 In this section, 18 takeoffs are treated as independent observations despite these being recorded
 161 on 9 individual birds. Indeed, the weather, the wind, the state of the sea, the moment, and the
 162 fishing area were uncontrolled and different from one flight to another (Fig. 2b).

163 (a) Parametric model estimation

164 The linear parametric models about each gull's elevation dynamics were estimated with the
 165 System Identification Toolbox from the Matlab software (parameters : time constant τ_h and static
 166 gain $\frac{1}{\omega_{sp}}$ in (5.2). The maximum climbing speed V_{zmax} (5.1) was computed from [24, 48]:

$$V_{zmax} = \frac{2.16 \cdot m_m \cdot f}{m} - \frac{1.92 \cdot m^{\frac{2}{3}}}{\rho^{\frac{1}{2}} \cdot b^{\frac{3}{2}}} \quad (5.1)$$

167 where m_m is the mass of the flight muscles, f is the observed flapping frequency (3.26 Hz on
 168 average, see page 162 in [17]), m is the total mass including any added load, ρ is the air density
 169 (1.205 kg/m^3 at 20°C) and b is the wing span. The vertical wind is low over the sea, consequently

170 in flight, we neglected the vertical wind. For each of the 18 offshore takeoffs followed by a cruise
171 flight, we took into account the morphological parameters of each gull.

172 (b) Computation of the predicted altitude

173 The model output, i.e. the predicted altitude, h_{est} , was computed with the Simulink environment
174 from the Matlab software. The best fit factor of the optic flow-based control model is obtained
175 by adjusting the flight muscle fraction ($\frac{m_m}{m}$) instead of the bird mass m , because the bird mass
176 was known without any prey load. The fit factor considered was the goodness of fit between
177 optimized simulated data (h_{est}) and actual GPS data (h_{GPS}) using a Matlab function with a
178 normalized mean square error cost function (called NRMSE cost function). NRMSE fit factor
179 varies between minus infinity (worse fit) to 1 (perfect fit). According to the table 15 in [21], the
180 flight muscle ratio ($\frac{m_m}{m}$) is relatively constant across birds species at 0.18 ± 0.05 (MEAN \pm SD,
181 with $n = 221$). Our simulated model has been adjusted with the flight muscle ratio in order to get
182 the best fit factor, then adjusting the maximum climbing speed in the elevation dynamics model.
183 For our group of 9 individual lesser black-backed gulls, we obtained the best fit factor with a
184 corresponding distribution of flight muscle ratio ($\frac{m_m}{m}$) of 0.18 ± 0.03 , which is quite similar
185 to prediction 9 from [24]. The optic flow-based control model takes into account the observed
186 correlation between the groundspeed V_g and the altitude h coming from gulls' GPS data. The
187 proportionality factor is called here a ventral optic-flow set-point ω_{sp} (2.6). Once the best fit factor
188 has been reached by adjusting the flight muscle fraction $\frac{m_m}{m}$, each gull's altitude is re-computed
189 by considering an altitude control model that directly feeds the elevation dynamics with a "target
190 flight altitude", noted an altitude set-point h_{sp} , which is computed when the gull reached its
191 steady-state altitude.

192 (c) Optic flow-based altitude control model

193 We consider two scales of time. The gull's forward dynamics responds faster than the gull's
194 upward dynamics (constrained by V_{zmax} see (5.1)) because the height of flight arises from the
195 response of a first order differential equation by considering the forward speed as a step input
196 (5.2). The bird's elevation dynamics is represented in Fig. 5a, this includes both the first order
197 upward dynamics (5.2) and the maximum climbing speed V_{zmax} (5.1).

$$\tau_h \cdot \frac{dh}{dt} + h(t) = \frac{1}{\omega_{sp}} \cdot V_g(t) \quad (5.2)$$

198 An explicit solution of equation (5.2) can be written, if we consider a step response at a given
199 positive amplitude V_{g0} value, as follows:

$$h(t) = \frac{V_{g0}}{\omega_{sp}} \cdot \left(1 - e^{-\frac{t}{\tau_h}}\right) \quad (5.3)$$

200 For each gull trajectory, we consider only one takeoff followed by a cruise flight, and then
201 we perform a first order system identification described by the differential equation (5.2). In this
202 model, a proportionality factor $\frac{1}{\omega_{sp}}$ is introduced, which is the inverse of the ventral optic-flow
203 set-point ω_{sp} (2.6), and the input of the upward dynamics (5.2) is the groundspeed V_g , which
204 correlates the altitude h and the groundspeed V_g . If the gull's groundspeed is constant during
205 takeoff as well as during cruising flight, then the predicted altitude profile will be the same with
206 both models.

207 The inter-flight variability of the climb time constant ($\tau_h = 97.3s \pm 68.0s$, with $n = 18$ takeoffs)
208 was derived on the basis of morphological properties of the birds (*inter alia* age, wingspan, body
209 mass including the load of prey and sex).

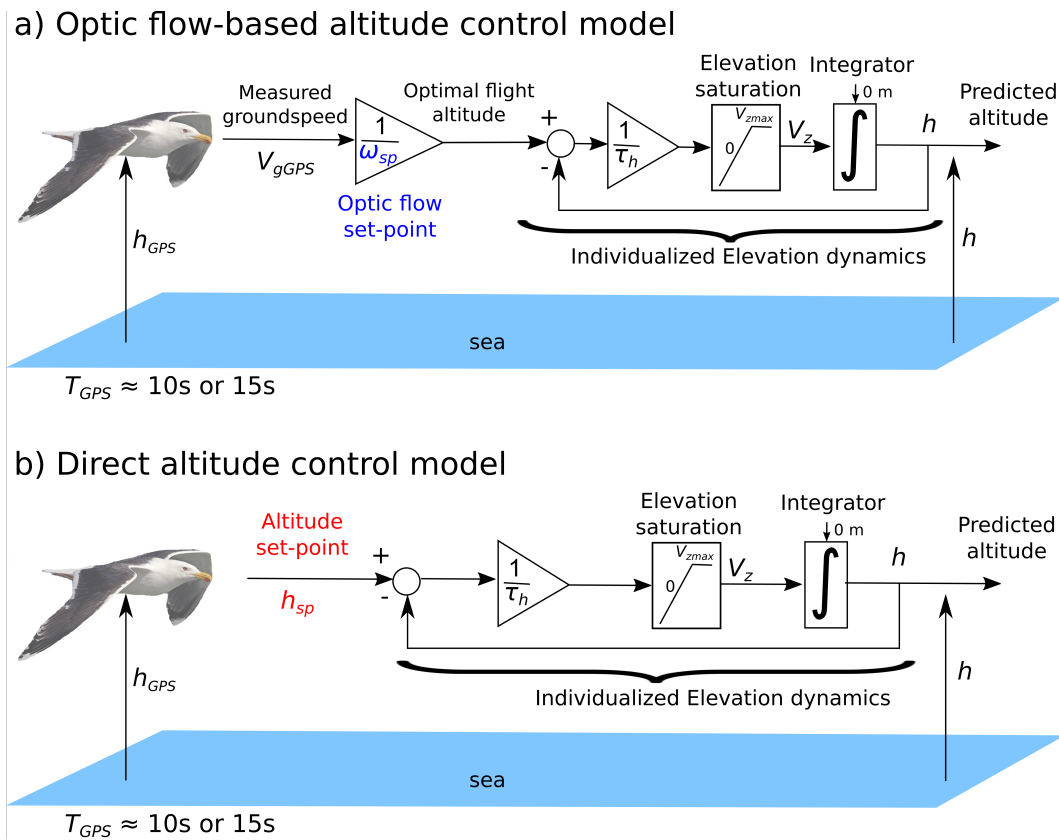


Figure 5. (a) Optic flow-based altitude control model including an individualized gull's elevation dynamics. Once the gull has reached the minimum groundspeed to takeoff, groundspeed is then relatively constant during its flight, an optic-flow-based control system can be switched on and lead the gull to a given altitude depending on both its groundspeed V_g and its ventral optic flow set-point ω_{sp} . The ventral optic-flow set-point ω_{sp} is an internal parameter used by the gull to tend asymptotically to its optimal flight altitude proportionally to its current groundspeed V_g . This model correlates the gull's current groundspeed to its current altitude. (b) Direct altitude control model. Here, the model only includes an individualized elevation dynamics and an altitude set-point h_{sp} . This model does not impose asymptotically any proportionality between groundspeed and altitude. The altitude set-point h_{sp} is an internal parameter used by the gull to select its "desired" or "target" flight altitude.

210 (d) Direct altitude control model

211 Here, the bird's elevation dynamics is represented in Fig. 5b, which includes both the first order
 212 upward dynamics (5.4) and the maximum climbing speed V_{zmax} (5.1).

$$\tau_h \cdot \frac{dh}{dt} + h(t) = h_{sp} \quad (5.4)$$

213 An explicit solution of equation (5.4) can be written, if we consider a step response at a given
 214 altitude h_{sp} value, as follows:

$$h(t) = h_{sp} \cdot \left(1 - e^{-\frac{t}{\tau_h}}\right) \quad (5.5)$$

215 The "target flight altitude", also called the altitude set-point is denoted h_{sp} , which is computed
 216 from when the gull reached its steady-state altitude, i.e. the gull's mean altitude when $t > 3\tau_h$ or
 217 $t > 5\tau_h$, depending on data availability. In this model, there is no correlation between altitude and
 218 groundspeed.

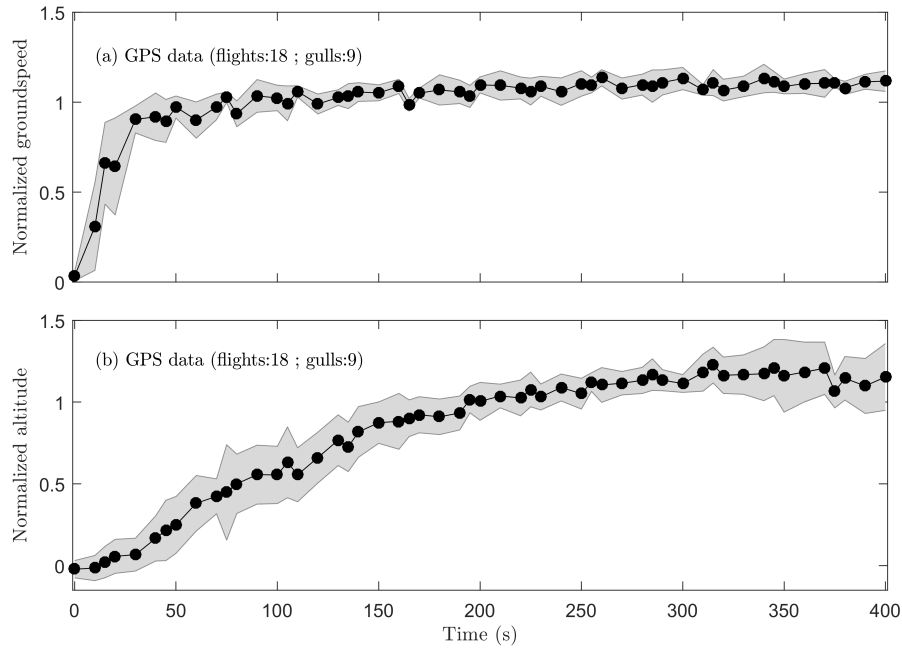


Figure 6. (a) Normalized groundspeed coming from GPS speed measurements $\frac{V_{gGPS}}{\text{mean}(V_{gGPS})}$, which is computed by the current groundspeed to average groundspeed ratio. (b) Normalized altitude coming from GPS data, which is computed by the current altitude to average altitude (by removing the first 100 seconds) ratio $\frac{h_{GPS}}{\text{mean}(h_{GPS}(100s:end))}$. Black dots represent GPS data recorded at a sampling time 10 s (12 trajectories) or 15 s (6 trajectories). Each dot represents the median value and shaded areas represent the median absolute deviation (MAD) of the GPS data collected from 18 flights.

219 (e) Comparison between optic flow-based and direct altitude control
220 models

221 A set of 18 trajectories representing 9 different gulls are individually shown in the horizontal
222 plane in Fig. 2b. The set of GPS data are clustered and shown in Fig. 6 for the initial 400 seconds
223 of each flight. It allows us not only to show the increase in speed during the gulls takeoff (Fig. 6a),
224 but also their level flight along the vertical plane (Fig. 6b). Both groundspeed and altitude have
225 been individually normalized by the steady state value reached by the gull's groundspeed and
226 altitude, respectively (Fig. 6). Consequently, both curves reach a steady state close to a value of
227 one (Fig. 6).

228 A linear 1st order parametric model on the data (18 trajectories) gives a fit factor value
229 (i.e., a normalized mean square error cost function, called NRMSE cost function) of 40.4%
230 on average (range: 10-80%). Then, by introducing a constraint on the climb rate according to
231 prediction 10 in [24, 48], a direct altitude control model based on a non-linear 1st order parametric
232 model combined with an altitude set-point h_{sp} (see Fig. 5b for details) gives a fit factor of on
233 average 57.1% (range: 11-77%). However, by adding to the previous model a correlation between
234 groundspeed and altitude, which is linked to what we call an optic flow set-point ω_{sp} (see Fig.
235 5a for details), an optic flow-based control model gives a fit factor of 63.4% on average (range:
236 30-83%).

237 Examples comparing an optic flow-based control model to a direct altitude control model for
238 one takeoff is given in Fig. 7b (the 17 other takeoffs are shown in Supplemental Information, Figs.
239 S3-S19). We observe that in each case the fit factor was higher with an optic flow-based control
240 model (blue dots in Fig. 7b rather than a direct altitude control model (red dots in Fig. 7b).

241 The set of normalized predicted altitudes ($n = 18$) computed with an altitude control model
242 (Fig. 5b) is shown in Fig. 8a, and with an optic flow-based control model (Fig. 5b) is shown
243 in Fig. 8b. Residuals, which are the errors between altitudes coming from GPS data and
244 predicted altitudes coming from models, are represented in Figs. 8c-d. We compared the residuals
245 distribution between the two models in transient response (white shaded boxes in Fig. S2) and
246 in steady-state response (gray shaded boxes in Fig. S2). The median value of the residuals (Figs.
247 8c-d) coming from the optic flow-based model was significantly higher in transient response (one-
248 sided Wilcoxon rank sum test, $n = 27$, $p \ll 0.001$) and was also significantly higher in steady-state
249 response (one-sided Wilcoxon rank sum test, $n = 27$, $p \ll 0.001$). Consequently for both parts, the
250 response predicted by the optic flow-based control model was better than the response predicted
251 by the altitude control model. Finally, the average value of the residuals coming from each
252 control model in transient response, then in steady-state response, were compared to a normal
253 distribution centred around zero. The distributions of residuals with the optic flow-based control
254 model (white shaded boxes in Fig. S2) were not significantly different from a normal distribution
255 centred around zero (t -test, $n = 27$, $p = 0.95$ in transient response, and $p = 0.07$ in steady-state
256 response). Residuals with the direct altitude control model (gray shaded boxes in Fig. S2) were
257 significantly different from a normal distribution centred around zero (t -test, $n = 27$, $p < 0.01$ in
258 transient response and $p \ll 0.001$ in steady-state response). This statistical analysis shows that the
259 optic flow-based control model is the most established model. Besides, for 13 out of 18 flights,
260 we observe a significant correlation (Spearman's test on GPS data) between groundspeed and
261 altitude (ρ from 0.22 to 0.83, 13 flights). We therefore conclude that our optic flow-based control
262 model (Fig. 5a) better explains the gulls' GPS tracking data than the direct altitude control model
263 (Fig. 5b).

264 6. Discussion

265 (a) Comparison of optic flow set-points identified by both analyses

266 We compared the distribution of ventral optic flow set-points coming from the tuned parametric
267 model obtained from the takeoff time series ($\omega_{sp} = 22^\circ/s \pm 9^\circ/s$ with $n = 18$, Shapiro normality
268 test: $p = 0.16$) and the parameter $\omega_{sp-lmer} = 25.23^\circ/s$ obtained from the linear mixed effect
269 model (4.2), respectively. No significant difference was observed between the ω_{sp} distribution
270 and the value $\omega_{sp-lmer}$ (t -test, $t:1.5296$, $df: 16$, p -value:0.1457). This suggests shows that both
271 analyses identify optic-flow set-points that are in the same range and not significantly different.
272 As a consequence, both the takeoff time-series and the full dataset support the ventral optic flow
273 regulation hypothesis in a consistent manner.

274 (b) Effect of wind on the birds' altitude

275 An additional outcome of the ventral optic flow regulation hypothesis [18, 55] is that any increase
276 in headwind will lead to a decrease in gull flight altitude in order to maintain the ventral optic
277 flow constant (Fig. 9a). Conversely, any increase in tailwind will lead to an increase in bird altitude
278 (Fig. 9c). A bird can adjust its ground speed by adjusting its airspeed or its heading relative
279 to ground (and wind), thus allowing it to minimize its cost of transport in flight. The altitude
280 control system based on optic flow is therefore consistent with previous observations on speed
281 adjustment with respect to winds in migrating birds [2].

282 The small Hellman exponent α over relatively smooth surfaces, such as the sea, means that
283 wind speed increases more rapidly than over a rough surface (e.g. a forest). Thus at higher
284 altitudes (i.e., from 10 m to 100 m) wind speed will not vary much, but below 10 m wind speed
285 can double going from 1 m to 10 m. Around the sea's waves wind is deflected leading to a pattern
286 of updrafts and downdrafts [50, 53, 68]. Together these effects are used by soaring seabirds in
287 dynamic soaring, gust soaring or "sweeping flight" [50, 53, 68], and the characteristic meandering
288 flight style that results has been termed "wave-meandering wing-sailing" [61]. Flapping seabirds

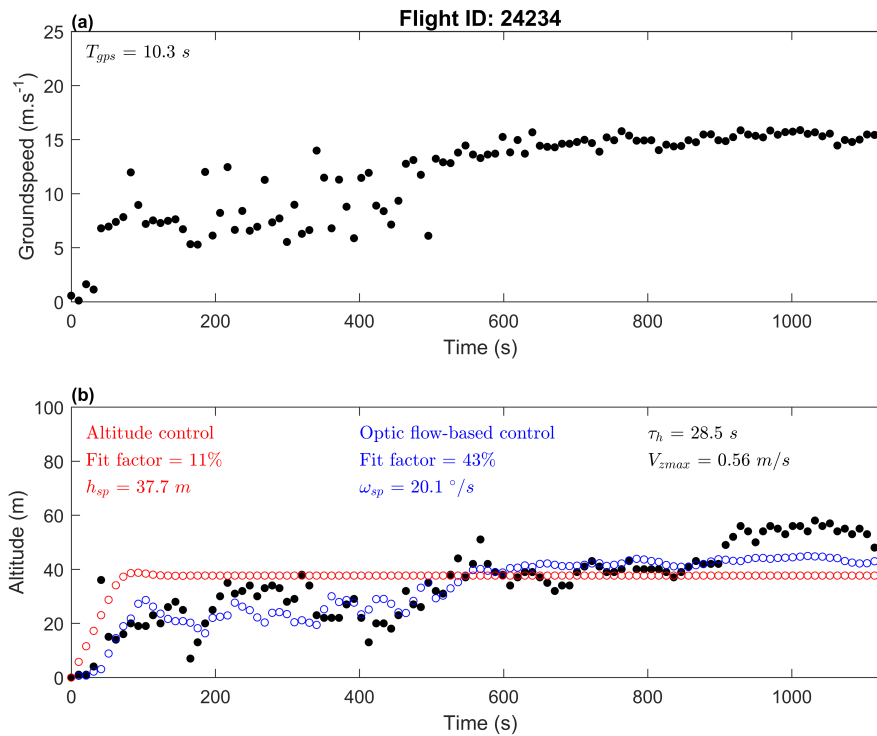


Figure 7. (a) Groundspeed of the gull ID24234 tracked with the GPS. (b) Altitude of the gull: black dots represent the GPS data, red dots represent the gull altitude on the basis of an altitude-based control model (fit factor: 11%), and the blue dots represent the gull altitude on the basis of an optic flow-based control model (fit factor: 43%). A significant correlation was observed between groundspeed and altitude of the GPS data ($\rho = 0.83$, $p \ll 0.001$ by Spearman's test).

289 can also use these features to gain a higher climb rate at the start of a take-off maneuver, taking
 290 off facing into the wind in the updraft formed by the deflection of the wind over a wave (see
 291 page 268 in [51], and [33]), which therefore reduces the effort required to take-off and accelerate
 292 to reach the maximum range speed V_{mr} . Seabirds may also use the "ground effect" while flying
 293 very close to the sea to reduce their energetic expenditure [8], which is helpful for takeoff at sea.

294 (c) Effect of altitude on optic flow

295 According to prediction 3 in [24, 48], the optimal altitude for a migratory bird is that where it can
 296 get just sufficient oxygen to maintain its cruising airspeed. This arises from the power required to
 297 fly at maximum range speed decreasing with altitude due to decreasing air density. Consequently,
 298 at an altitude of 6000 m, where the air density is half that at sea level, a bird should theoretically
 299 fly $\sqrt{2}$ times faster. On the other hand, at a given optic-flow set-point working in a 100 m altitude
 300 range, the optic flow would be divided by a factor $\frac{60}{\sqrt{2}}$ at an altitude of 6000 m. Therefore the optic
 301 flow would be too small to be maintained at the amplitude of the one generated in a 100 m altitude
 302 range. Recently, McLaren and colleagues (2016) analysing flights of lesser black-backed gulls
 303 flying between south-east England and The Netherlands recorded much greater flight altitudes
 304 than those observed here during homing flights to the breeding colony, with maximal values 1,240
 305 m [42], even though typical values were lower at 100-150 m. On migratory flights, the gulls have
 306 been recorded flying higher still, though that is overland, with maximal altitudes around 5,000
 307 m (unpublished data). Consequently, an optic flow based altitude control system can only work

308 below a 100-meter altitude range where the optic flow is significant and detectable by the visual
309 system of the birds.

310 (d) Are groundspeed and altitude still proportional at higher altitudes?

311 Birds making lower altitude flights (<100-150 m) will generate a detectable optic flow. However,
312 when on long distance or migratory flights birds may fly higher at hundreds to thousands of
313 meters (see above), optic flow values will then be extremely low, thus unlikely to be suitable for
314 regulating a given optic flow set-point. This relates to the finding for common swifts (*Apus apus*)
315 by Hedenström & Åkesson (2017), that the swifts did not compensate for head- and tail winds as
316 expected from flight mechanical theory when flying at high altitudes (>1000 m), but they did so at
317 low altitudes (<100 m) [25]. This was interpreted as a failure to detect small changes in optic flow
318 due to winds by the swifts' visual system at high altitudes. In addition, for altitudes higher than
319 400 m, lesser black-backed gulls were observed to compensate less for cross-wind disturbance
320 than they did at lower altitudes: fractional compensations were observed to decrease from about
321 1.3 (on average) to less than 0.5 at 900 m height [42]. At altitudes above 400 m, gulls' groundspeed
322 may be highly dependent on the wind speed: no altitude increase or decrease can be predicted
323 with respect to the optic flow-based control model as optic flow is low thus its changes with
324 altitude would be difficult to detect by the gulls' visual system.

325 (e) Bird navigation in the vertical dimension: can birds use barometric 326 pressure to determine altitude?

327 The birds' mechanoreceptive paratympanic organ (PTO) is located in the middle ear, and it is
328 probably used by birds to detect barometric pressure [65]. Birds appear to use the PTO not only
329 as a barometer to predict the onset of inclement weather [10, 60, 65], but also as a genuine altimeter
330 to adjust their flight altitude during migration. Birds can fly level within ± 20 m for distances of
331 2–3km at altitudes of 700 – 1,100m, even at night [22], i.e. without visual cues. However, it is still
332 an open question whether birds can use changing barometric pressure directly to measure their
333 current altitude in real time.

334 A mechanoreceptive scale sensory organ found in fish [5] may play the same sensory function
335 as the PTO in birds. It is known that fish can determine their depth using hydrostatic pressure
336 [29, 63]. On this point, it was demonstrated that the dynamic depth sensing in fish is less than 1
337 m at a depth of 100 m [63]. However, water density is approximately 1,000 times higher than air
338 density, and the pressure gradient in flight is therefore particularly low generating extremely low
339 frequencies in the feedback signal to the bird's elevation dynamics. Therefore, it would be difficult
340 to adjust the flight altitude for a short period of time, only being practical for long periods of time
341 such as for example during longer distance migratory flights.

342 (f) Effect of wave motion on the optic flow pattern

343 The flight model assumes that the sea-surface, over which the gulls fly, provides a stationary
344 reference frame: no data are currently available on the wave speed. Therefore, the optic flow
345 experienced by the gulls is solely modeled as a function of their own movement (groundspeed
346 and altitude). Previous studies on bird navigation over water suggest that the seascape (or more
347 specifically the wavescape) is not a fixed reference frame [1], as the wave patterns move, usually
348 in roughly the same direction as the wind but at a slower speed. Therefore the perceived optic
349 flow will be different than the physical optic flow. Alerstam & Petterson (1976) suggested that the
350 motion of the wave scape allows birds to only partially compensate for wind-drift over the sea
351 [3], thus presumably a similar constraint may apply to using the ventral optic flow for control of
352 flight altitude.

353 Overall, the wave pattern will reduce the adjustment of altitude if a fixed optic flow set-point
354 was used, as under headwinds perceived optic flow will be higher than otherwise, i.e. even

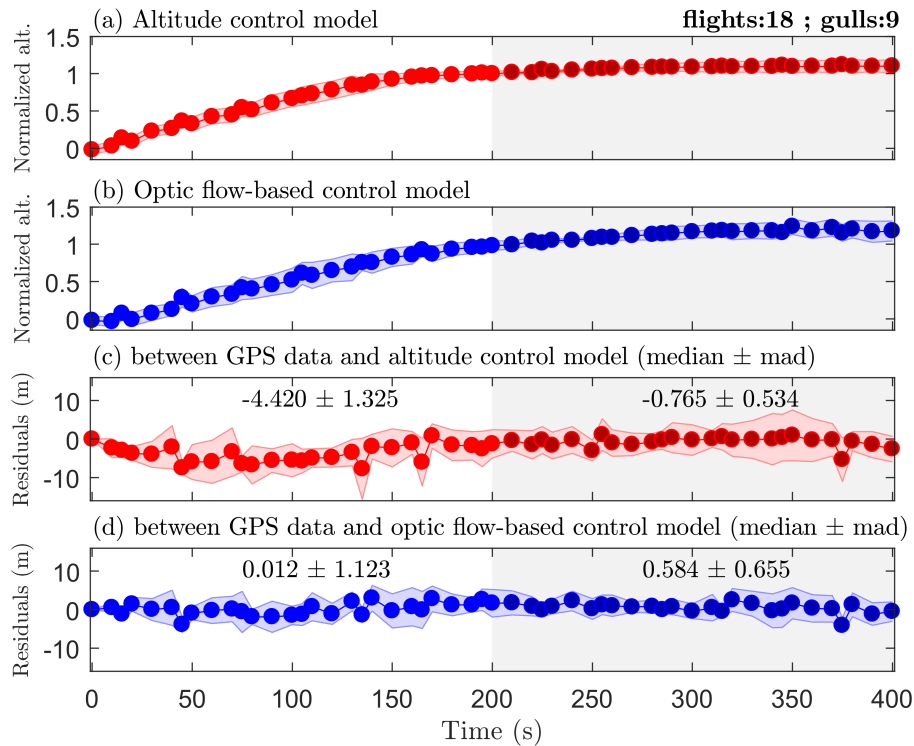


Figure 8. Red dots (altitude control model) or blue dots (optic flow-based control model) represent predicted altitude ((a) and (b)) or residuals ((c) and (d)) at a same sampling time 10 s (12 trajectories) or 15 s (6 trajectories) like GPS data (see Fig. 6). Each dot represents the median value and shaded areas represent the median absolute deviation (MAD) of data ($n = 18$). The white shaded areas represent the transient response (time < 200 s) during takeoff and ascent, and the gray shaded areas represent the steady state response (time > 200 s) once in cruising flight. The duration $200 \text{ s} \approx 2 \cdot \tau_h$ represents about 86% of the step response of a 1st order dynamic system (see (5.3)). (a) Normalized predicted altitude using an **altitude control model** (Fig. 5b), which is computed by current predicted altitude average predicted altitude (by removing the first 100 seconds) ratio $\frac{h}{\text{mean}(h(100s:end))}$. (b) Normalized predicted altitude using an **optic flow-based control model** (Fig. 5a), which is computed by current predicted altitude average predicted altitude (by removing the first 100 seconds) ratio $\frac{h}{\text{mean}(h(100s:end))}$. (c) Residuals between GPS data (Fig. 6b) and altitude computed with the altitude control model (data in (a)). (d) Residuals between GPS data (Fig. 6b) and altitude computed with the optic-flow based control model (data in (b)).

355 as groundspeed approaches zero there will still be a perceived optic flow if the wavescape is
 356 moving, which would lead to higher flight altitudes than expected. While under tailwinds optic
 357 flow is somewhat reduced, as the sea surface pattern will be moving in the same direction as the
 358 bird, and hence lower than expected flight altitudes would result. The wave pattern distorts the
 359 ventral optic flow perceived: such disturbances could be added to the flight model once data or a
 360 methodology of how to obtain wave pattern becomes available.

361 However, for optic flow to be useful ripples above the sea are essential to form a textured
 362 surface. In fact, it was observed by Heran & Lindauer (1963) that a great number of honeybees
 363 plunged into the water when the water surface was mirror smooth [28]. An altitude control
 364 system based solely on a ventral optic flow regulation irrevocably pulls any flying animal down
 365 whenever its eye fails to measure an optic flow [18]. This did not happen in honeybees when the
 366 water surface was rippled [28, 62] or when a floating bridge provided a visual contrast [28].

367 At this level of reasoning, we may wonder if the visual pattern produced by waves was
 368 textured enough during the gulls' flights for an optic flow field to be perceived. To investigate

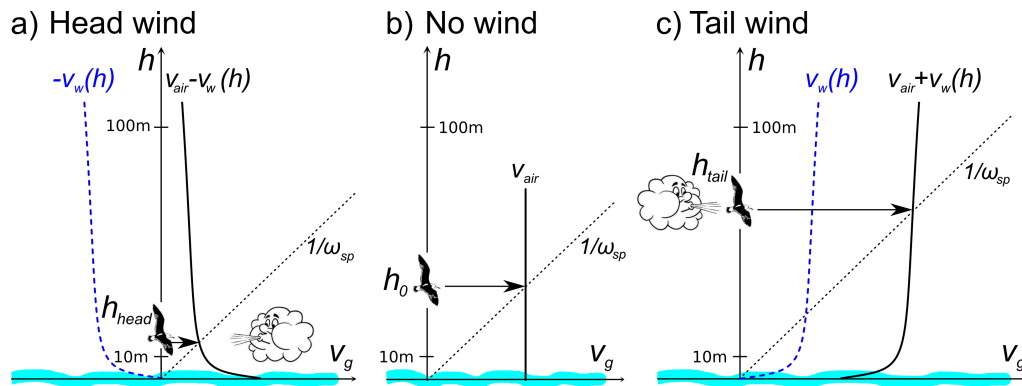


Figure 9. Gull's speed and altitude for three different wind scenarios under the hypothesis that the gull adjusts its vertical lift to maintain constant its ventral optic flow. The red straight line $\frac{1}{\omega_{sp}}$ indicates the set of possible pairs of altitudes and groundspeeds allowed by the ventral optic flow regulation hypothesis. (a) In the presence of a head wind, given that the wind speed increases with the altitude, the groundspeed profile $V_{air} - V_w(h)$ intersects the straight line $\frac{1}{\omega_{sp}}$ at a lower altitude h_{head} than in absence of wind. (b) In the absence of wind, the ground speed and hence the altitude depend only on the airspeed produced by the agent: the vertical line $V_g = V_{air}$ intersects the line $\frac{1}{\omega_{sp}}$ at the altitude h_0 . (c) In the presence of a tail wind, the ground speed profile $V_{air} + V_w(h)$ intersects the straight line $\frac{1}{\omega_{sp}}$ at a greater altitude h_{tail} than in absence of wind. Modified from [55].

369 this, knowing that the average significant wave height of the Baltic Sea in 1991–2015 was in the
 370 range 0.44–1.94 m [34], which corresponds to a Beaufort number of 3 (gentle breeze, mean wind
 371 speed equivalent from 3.4 m/s to 5.4 m/s) to 4 (moderate breeze, mean wind speed equivalent
 372 from 5.5 m/s to 7.9 m/s) [6]. We deduce that gulls could see scattered or fairly frequent white-
 373 crested waves at an effective height of 10 m above the sea level. However for Beaufort numbers
 374 from 0 to 2, the sea has a smooth appearance, which makes for poor visual conditions to perceive
 375 an optic flow field. Interestingly, the wind conditions corresponding to a Beaufort number from 3
 376 to 4 fit not only with the wind conditions of gulls in flight (Fig. S20), but also with their altitude
 377 (see page 166 in [17]). We can conclude that wind is an important parameter to generate an optic
 378 flow field cue, and to help gulls to control their flight above the sea.

379 Little is known about the visual system of gulls. The spatial acuity of seabirds can be more
 380 than four times lower than that in humans [43], with a maximum spatial acuity of about 60
 381 cycles/degree in humans. Moreover, in seabirds rods are evenly distributed across the entire
 382 retina [15], which allow them to conveniently detect the optic flow coming from the sea. Most
 383 of the seabirds have a maximum binocular field width in the $15^\circ - 30^\circ$ range (about 120° in
 384 humans), which is limited, suggesting that binocular vision plays only a minor role in seabirds'
 385 flight control system [39]. We conclude that the optic flow field is the major visual cue used by
 386 seabirds to control their flight above the sea.

387 (g) Optic-flow set-point: differences between honeybees and gulls

388 There are a number of differences in flight behaviours expressed by birds and flying insects
 389 [4]. Typically, the average maximum airspeed of honeybees is approximately 7.5 m/s with a
 390 minimum power speed of their power U-curve at 3.3 m/s [44]. In free-flight natural conditions,
 391 honeybees have been observed to fly from 3.3 m/s to 5.1 m/s [44]. However, lesser black-backed
 392 gulls typically fly at an airspeed in natural offshore conditions at an average 12.3 m/s \pm 2 m/s
 393 (see [17], page 166) with a minimum power speed of their power U-curve at 9.3 m/s (computed
 394 for lesser black-backed gull, see [27]). Hence, lesser black-backed gulls can fly 3 times faster than
 395 honeybees by comparing their minimum power speed.

396 In honeybees, average maximal flight height is about 2.5 m over natural terrain [16, 28]. In
397 general, lesser black-backed gulls fly at an altitude over sea of up to 130 m with a distribution of
398 $31 \text{ m} \pm 29 \text{ m}$ on average (see [17], pages 166-167) during foraging flights. We conclude that lesser
399 black-backed gulls fly much higher than honeybees during foraging flights, which reduces optic
400 flow emanating from the sea.

401 Consequently, we can conclude from these two last points that the ventral optic-flow set-point
402 of lesser black-backed gulls is much lower than that typically experienced by honeybees, knowing
403 that the ventral optic-flow set-point of honeybees is close to $200^\circ/s$. Our statistical analysis
404 estimates that the ventral optic-flow set-point of lesser black-backed gulls is close to $25^\circ/s$ on
405 average (see section 4), which is a detectable value by the gulls' visual system [39, 40, 41]. A recent
406 review indicates that pigeons' fast LM neurons (pretectal nucleus lentiformis mesencephali)
407 respond to optic flow stimuli of their preferred backward direction (front to back visual stimuli:
408 temporal to nasal on the retina) in this same angular velocities range [69].

409 7. Conclusion

410 A mathematical model of optic flow-based offshore takeoff control system in lesser black-backed
411 gulls was developed in this study to understand what visual cue can be used by seabirds to
412 control their takeoff and to cruise over a sea surface. This mathematical model introduced an
413 optic flow set-point parameter, which aims to be maintained constant by seabirds during take-
414 off manoeuvres and cruising foraging flights. Besides, the model takes into account the bird's
415 individual morphology through its elevation dynamics. Finally, both analyses on the takeoff time-
416 series and the full dataset support the ventral optic flow regulation hypothesis in a consistent
417 manner.

418 We conclude that the optic-flow regulation principle allows seabirds to control their altitude
419 over sea at low flight altitudes without having to measure their current altitude directly by
420 another method. To do this, they just have to measure the optic flow perceived from the sea
421 to adjust their vertical thrust in order to maintain the ventral optic flow at a given value, called
422 the optic-flow set-point, as previously suggested for flying insects [18, 55]. According to both the
423 airspeed and altitude ranges of lesser black-backed gulls measured during flight in their natural
424 environment, we demonstrate that gulls could control their altitude by regulating the ventral
425 optic-flow at a value of $25^\circ/s$ on average, allowing them to fly jointly up to 130 m in altitude at
426 a groundspeed up to 20 m/s , while maintaining visual contact with the sea. The introduction of
427 this asymptotic proportionality relationship for birds also accounts very nicely for the transient
428 altitude response during takeoff. Overall, gulls need such accurate altitude control based on optic
429 flow to optimize their energetic effort irrespectively of favorable or unfavorable unknown wind
430 conditions while being robust to ground disturbances such as relief.

431 Authors' contributions

432 JRS, FR, TJE and AH developed the modelling; JRS ran the models on Matlab software; TJE and
433 SÅ tagged the gulls and collected the data; JRS, TJE and FR analysed the modelling results; JSB
434 provided the tracking system; FR and AH supervised the collaboration; FR drew figs 1 and 9; TJE
435 drew figs 2 and 3; JRS drew figs 5, 6, 7, 8 and S1-S19; TJE, JRS and FR drew fig 4; JRS wrote the
436 first draft of the paper; all authors prepared and revised the manuscript.

437 Acknowledgement

438 French financial support was provided by a project grant to FR from the CNRS PEPS
439 Avimod (Exomod Program). FR and JRS were also supported by Aix Marseille Université and
440 CNRS (Life Science; Information Science, and Engineering Science and Technology). Financial
441 support was via project grants to SÅ and AH from the Swedish Research Council (621-
442 2007-5930; 621-2010-5584, 621-2013-4361, 621-2012-3585) and Lund University, and a Linnaeus

443 grant from the Swedish Research Council (349-2007-8690) to the Centre for Animal Movement
444 Research (CAnMove) and Lund University. Field work was partly supported by WWF
445 Sweden. UvA-BiTS is facilitated by infrastructures for eScience, developed with support of the
446 NLeSC (<http://www.esciencecenter.com/>) and LifeWatch, carried out on the Dutch national e-
447 infrastructure with support of SURF Foundation. Permissions to capture and ring birds were
448 from the Swedish Nature Protection Board (Naturvårdsverket) and the Swedish Ringing Office
449 at the Natural History Museum in Stockholm. Ethical permission to tag the gulls was from
450 Malmö/Lund Djurförsöksetiska nämnd (No. M112-09, M470-12). Permission to work in the
451 protected area was from the county administration Länsstyrelsen Gotlands Län. For assistance
452 during fieldwork we thank the whole Baltic Seabird Group team, especially: Olof Olsson, Jonas
453 Hentati-Sundberg, Per-Arvid Berglund, Aron Hejdström, Martina Kadin, Natalie Isaksson, and
454 Rebecca Young. We would like to thank Prof. Maan El Badaoui El Najjar (Univ. of Lille) for his
455 fruitful comments during this analysis.

456 References

- 457 1 Åkesson, S. & Hedenström, A. 2007 How migrants get there: migratory performance and
458 orientation. *AIBS Bulletin*, **57**(2), 123–133.
- 459 2 Alerstam, T. 1990 *Bird migration*. Cambridge University Press.
- 460 3 Alerstam, T. & Pettersson, S.-G. 1976 Do birds use waves for orientation when migrating across
461 the sea? *Nature*, **259**(5540), 205–207.
- 462 4 Altshuler, D. L. & Srinivasan, M. V. 2018 Comparison of visually guided flight in insects and
463 birds. *Frontiers in neuroscience*, **12**, 157.
- 464 5 Baker, C. V., O'Neill, P. & McCole, R. B. 2008 Lateral line, otic and epibranchial placodes:
465 developmental and evolutionary links? *Journal of Experimental Zoology Part B: Molecular and*
466 *Developmental Evolution*, **310**(4), 370–383.
- 467 6 Beaufort, F. 1805 Beaufort wind scale. *British Rea-Admiral*.
- 468 7 Bhagavatula, P. S., Claudianos, C., Ibbotson, M. R. & Srinivasan, M. V. 2011 Optic flow cues
469 guide flight in birds. *Current Biology*, **21**(21), 1794–1799.
- 470 8 Blake, R. 1985 A model of foraging efficiency and daily energy budget in the black skimmer
471 (*rynchops nigra*). *Canadian journal of zoology*, **63**(1), 42–48.
- 472 9 Bouten, W., Baaij, E. W., Shamoun-Baranes, J. & Camphuysen, K. C. 2013 A flexible gps
473 tracking system for studying bird behaviour at multiple scales. *Journal of Ornithology*, **154**(2),
474 571–580.
- 475 10 Breuner, C. W., Sprague, R. S., Patterson, S. H. & Woods, H. A. 2013 Environment, behavior
476 and physiology: do birds use barometric pressure to predict storms? *Journal of Experimental*
477 *Biology*, **216**(11), 1982–1990.
- 478 11 Coulson, J. C., Thomas, C. S., Butterfield, J. E. L., Duncan, N., Monaghan, P. & Shedden, C.
479 The use of head and bill length to sex live gulls larvae. *Ibis*, **125**(4), 549–557. (doi:10.1111/j.
480 1474-919X.1983.tb03148.x)
- 481 12 Davies, M. & Green, P. 1990 Optic flow-field variables trigger landing in hawk but not in
482 pigeons. *Naturwissenschaften*, **77**(3), 142–144.
- 483 13 Dee, D. P., Uppala, S. M., Simmons, A. J., Berrisford, P., Poli, P., Kobayashi, S., Andrae, U.,
484 Balmaseda, M. A., Balsamo, G. *et al.* 2011 The ERA-Interim reanalysis: configuration and
485 performance of the data assimilation system. *Quarterly Journal of the Royal Meteorological*
486 *Society*, **137**(656), 553–597. (doi:10.1002/qj.828)
- 487 14 Dodge, S., Bohrer, G., Weinzierl, R., Davidson, S. C., Kays, R., Douglas, D., Cruz, S., Han,
488 J., Brandes, D. *et al.* 2013 The environmental-data automated track annotation (Env-DATA)
489 system: linking animal tracks with environmental data. *Movement Ecology*, **1**(1), 3. (doi:10.
490 1186/2051-3933-1-3)
- 491 15 Emond, M., McNeil, R., Cabana, T., Guerra, C. & Lachapelle, P. 2006 Comparing the retinal
492 structures and functions in two species of gulls (*larus delawarensis* and *larus modestus*) with
493 significant nocturnal behaviours. *Vision research*, **46**(18), 2914–2925.

- 494 16 Esch, H. & Burns, J. 1996 Distance estimation by foraging honeybees. *Journal of Experimental*
495 *Biology*, **199**(1), 155–162.
- 496 17 Evans, T. J. 2017 *Across landscapes and seascapes : The movement ecology of diving and flying*
497 *guillemots and gulls during breeding*. PhD thesis, Lund University, Faculty of Science,
498 Department of Biology.
- 499 18 Franceschini, N., Ruffier, F. & Serres, J. 2007 A bio-inspired flying robot sheds light on insect
500 piloting abilities. *Current Biology*, **17**(4), 329–335.
- 501 19 Gibson, J. J. 1966 *The senses considered as perceptual systems*. Houghton Mifflin.
- 502 20 Goller, B. & Altshuler, D. L. 2014 Hummingbirds control hovering flight by stabilizing visual
503 motion. *Proceedings of the National Academy of Sciences*, **111**(51), 18 375–18 380.
- 504 21 Greenewalt, C. H. 1962 Dimensional relationships for flying animals. *Smithsonian miscellaneous*
505 *collections*, **144**, 1–46.
- 506 22 Griffin, D. R. 1969 The physiology and geophysics of bird navigation. *The Quarterly Review of*
507 *Biology*, **44**(3), 255–276.
- 508 23 Griffiths, R., Double, M. C., Orr, K. & Dawson, R. J. G. 1998 A DNA test to sex most birds.
509 *Molecular Ecology*, **7**(8), 1071–1075. (doi:10.1046/j.1365-294x.1998.00389.x)
- 510 24 Hedenström, A. 2003 Twenty-three testable predictions about bird flight. In *Avian migration*,
511 pp. 563–582. Springer.
- 512 25 Hedenström, A. & Åkesson, S. 2017 Adaptive airspeed adjustment and compensation for wind
513 drift in the common swift: Differences between day and night. *Animal Behaviour*, **127**, 117–123.
- 514 26 Hedenstrom, A. & Alerstam, T. 1995 Optimal flight speed of birds. *Philosophical Transactions of*
515 *the Royal Society of London B: Biological Sciences*, **348**(1326), 471–487.
- 516 27 Heerenbrink, M. K., Johansson, L. & Hedenström, A. 2015 Power of the wingbeat: modelling
517 the effects of flapping wings in vertebrate flight. *Proceedings of the Royal Society A*, **471**(2177),
518 20140952.
- 519 28 Heran, H. & Lindauer, M. 1963 Windkompensation und seitenwindkorrektur der bienen beim
520 flug über wasser. *Zeitschrift für vergleichende Physiologie*, **47**(1), 39–55.
- 521 29 Holbrook, R. I. & de Perera, T. B. 2011 Fish navigation in the vertical dimension: can fish use
522 hydrostatic pressure to determine depth? *Fish and Fisheries*, **12**(4), 370–379.
- 523 30 Hsu, S., Meindl, E. A. & Gilhousen, D. B. 1994 Determining the power-law wind-profile
524 exponent under near-neutral stability conditions at sea. *Journal of Applied Meteorology*, **33**(6),
525 757–765.
- 526 31 Irwin, J. S. 1979 A theoretical variation of the wind profile power-law exponent as a function
527 of surface roughness and stability. *Atmospheric Environment (1967)*, **13**(1), 191 – 194. (doi:[https://doi.org/10.1016/0004-6981\(79\)90260-9](https://doi.org/10.1016/0004-6981(79)90260-9))
- 528
529 32 Isaksson, N., Evans, T. J., Shamoun-Baranes, J. & Åkesson, S. 2016 Land or sea? Foraging
530 area choice during breeding by an omnivorous gull. *Movement Ecology*, **4**, 11. (doi:10.1186/
531 s40462-016-0078-5)
- 532 33 Kogure, Y., Sato, K., Watanuki, Y., Wanless, S. & Daunt, F. 2016 European shags optimize their
533 flight behavior according to wind conditions. *Journal of Experimental Biology*, **219**(3), 311–318.
- 534 34 Kudryavtseva, N. & Soomere, T. 2017 Satellite altimetry reveals spatial patterns of variations
535 in the baltic sea wave climate. *arXiv preprint arXiv:1705.01307*.
- 536 35 Lee, D. N. & Kalmus, H. 1980 The optic flow field: the foundation of vision. *Philosophical*
537 *Transactions of the Royal Society of London B: Biological Sciences*, **290**(1038), 169–179.
- 538 36 Lee, D. N. & Reddish, P. E. 1981 Plummeting gannets: a paradigm of ecological optics. *Nature*,
539 **293**(5830), 293–294.
- 540 37 Lee, D. N., Reddish, P. E. & Rand, D. 1991 Aerial docking by hummingbirds.
541 *Naturwissenschaften*, **78**(11), 526–527.
- 542 38 Liechti, F. 2006 Birds: blowin? by the wind? *Journal of Ornithology*, **147**(2), 202–211. (doi:10.
543 1007/s10336-006-0061-9)
- 544 39 Martin, G. R. 2009 What is binocular vision for? a birds' eye view. *Journal of Vision*, **9**(11), 14–14.
- 545 40 Martin, G. R. 2011 Understanding bird collisions with man-made objects: a sensory ecology
546 approach. *Ibis*, **153**(2), 239–254.

- 547 41 Martin, G. R. 2017 *The sensory ecology of birds*. Oxford University Press.
- 548 42 McLaren, J. D., Shamoun-Baranes, J., Camphuysen, C. & Bouten, W. 2016 Directed flight and
549 optimal airspeeds: homeward-bound gulls react flexibly to wind yet fly slower than predicted.
550 *Journal of Avian Biology*, **47**(4), 476–490.
- 551 43 Mitkus, M., Nevitt, G. A., Danielsen, J. & Kelber, A. 2016 Vision on the high seas: spatial
552 resolution and optical sensitivity in two procellariiform seabirds with different foraging
553 strategies. *Journal of Experimental Biology*, **219**(21), 3329–3338.
- 554 44 Nachtigall, W., Hanauer-Thieser, U. & Mörz, M. 1995 Flight of the honey bee vii: metabolic
555 power versus flight speed relation. *Journal of Comparative Physiology B: Biochemical, Systemic,
556 and Environmental Physiology*, **165**(6), 484–489.
- 557 45 Nakayama, K. & Loomis, J. 1974 Optical velocity patterns, velocity-sensitive neurons, and
558 space perception: a hypothesis. *Perception*, **3**(1), 63–80.
- 559 46 Orians, G. H. & Pearson, N. E. On the theory of central place foraging. In *Analysis of ecological
560 systems*. ohio state university press, columbus, pp. 155–177.
- 561 47 Pennycuick, C. 1975 Mechanics of flight. *Avian biology*, **5**, 1–75.
- 562 48 Pennycuick, C. J. 1978 Fifteen Testable Predictions about Bird Flight. *Oikos*, **30**(2), 165–176.
563 (doi:10.2307/3543476)
- 564 49 Pennycuick, C. J. 1989 *Bird flight performance*. Oxford University Press.
- 565 50 Pennycuick, C. J. 2002 Gust soaring as a basis for the flight of petrels and albatrosses
566 (Procellariiformes). *Avian Science*, **2**(1), 1–12.
- 567 51 Pennycuick, C. J. 2008 *Modelling the flying bird*, vol. 5. Elsevier.
- 568 52 Rayleigh 1883 The soaring of birds. *Nature*, **27**(701), 534–535. (doi:10.1038/027534a0)
- 569 53 Richardson, P. L. 2011 How do albatrosses fly around the world without flapping their wings?
570 *Progress in Oceanography*, **88**(1), 46–58.
- 571 54 Ros, I. G. & Biewener, A. A. 2016 Optic flow stabilizes flight in ruby-throated hummingbirds.
572 *Journal of Experimental Biology*, **219**(16), 2443–2448.
- 573 55 Ruffier, F. & Franceschini, N. 2005 Optic flow regulation: the key to aircraft automatic
574 guidance. *Robotics and Autonomous Systems*, **50**(4), 177–194.
- 575 56 Sachs, G., Traugott, J., Nesterova, A. P., Dell’Omo, G., Kummeth, F., Heidrich, W., Vyssotski,
576 A. L. & Bonadonna, F. 2012 Flying at no mechanical energy cost: disclosing the secret of
577 wandering albatrosses. *PLoS One*, **7**(9), e41449.
- 578 57 Schiffner, I. & Srinivasan, M. V. 2016 Budgerigar flight in a varying environment: flight at
579 distinct speeds? *Biology Letters*, **12**(6), 20160221.
- 580 58 Serres, J. R. & Ruffier, F. 2017 Optic flow-based collision-free strategies: From insects to robots.
581 *Arthropod Structure & Development*, **46**(5), 703–717.
- 582 59 Shamoun-Baranes, J., Liechti, F. & Vansteelant, W. M. 2017 Atmospheric conditions create
583 freeways, detours and tailbacks for migrating birds. *Journal of Comparative Physiology A*, pp.
584 1–21.
- 585 60 Shamoun-Baranes, J., Van Loon, E., Alon, D., Alpert, P., Yom-Tov, Y. & Leshem, Y. 2006 Is there
586 a connection between weather at departure sites, onset of migration and timing of soaring-bird
587 autumn migration in israel? *Global Ecology and Biogeography*, **15**(6), 541–552.
- 588 61 Spivey, R., Stansfield, S. & Bishop, C. 2014 Analysing the intermittent flapping flight of a manx
589 shearwater, *puffinus puffinus*, and its sporadic use of a wave-meandering wing-sailing flight
590 strategy. *Progress in Oceanography*, **125**, 62–73.
- 591 62 Tautz, J., Zhang, S., Spaethe, J., Brockmann, A., Si, A. & Srinivasan, M. 2004 Honeybee
592 odometry: performance in varying natural terrain. *PLoS Biology*, **2**(7), e211.
- 593 63 Taylor, G. K., Holbrook, R. I. & de Perera, T. B. 2010 Fractional rate of change of swim-bladder
594 volume is reliably related to absolute depth during vertical displacements in teleost fish.
595 *Journal of The Royal Society Interface*, **7**(50), 1379–1382.
- 596 64 Thaxter, C. B., Ross-Smith, V. H., Clark, J. A., Clark, N. A., Conway, G. J., Marsh, M., Leat,
597 E. H. & Burton, N. H. 2014 A trial of three harness attachment methods and their suitability
598 for long-term use on Lesser Black-backed Gulls and Great Skuas. *Ringing & Migration*, **29**(2),
599 65–76. (doi:10.1080/03078698.2014.995546)
- 600 65 von Bartheld, C. S. & Giannessi, F. 2011 The paratympanic organ: a barometer and altimeter
601 in the middle ear of birds? *Journal of Experimental Zoology Part B: Molecular and Developmental
602 Evolution*, **316**(6), 402–408.

- 603 66 Weimerskirch, H., Guionnet, T., Martin, J., Shaffer, S. A. & Costa, D. P. 2000 Fast and fuel
604 efficient? Optimal use of wind by flying albatrosses. *Proceedings of the Royal Society B: Biological*
605 *Sciences*, **267**(1455), 1869–1874. (doi:10.1098/rspb.2000.1223)
- 606 67 Whiteside, T. C. & Samuel, G. 1970 Blur zone. *Nature*, **225**(5227), 94–95.
- 607 68 Wilson, J. A. 1975 Sweeping flight and soaring by albatrosses. *Nature*, **257**(5524), 307. (doi:10.
608 1038/257307a0)
- 609 69 Wylie, D. R., Gutiérrez-Ibáñez, C., Gaede, A. H., Altshuler, D. L. & Iwaniuk, A. N. 2018 Visual-
610 cerebellar pathways and their roles in the control of avian flight. *Frontiers in Neuroscience*, **12**,
611 223. (doi:10.3389/fnins.2018.00223)